

In Situ Mechanical Characterization of Structural Bamboo Materials under Flexural Bending

J. Song^{1,2} · L. Gao¹ · Y. Lu^{1,3} 

Received: 13 February 2017 / Accepted: 2 August 2017 / Published online: 8 August 2017
© The Society for Experimental Mechanics, Inc 2017

Abstract Experimental mechanical characterization of structural biomaterials, coupled with advanced *in situ* microscopic imaging, is critical for understanding their deformation and failure mechanisms in engineering applications. Our earlier study suggested that bamboo materials, widely used as scaffolding in construction, exhibit superior and asymmetric bending flexural behavior, while their corresponding mechanisms for crack growth under bending are not fully understood due to the complicated hierarchical structure. Here, we developed *in situ* characterization techniques assisted with high-resolution macro telescope to directly observe the flexural responses of bamboo strips under different loading configurations. Our *in situ* results show that the hierarchical microstructure of bamboo plays a critical role in alternating the crack propagation behaviors as well as failure mechanisms. In addition, a finite element analysis (FEA) model mimicking bamboo's functional graded (FG) structure has been developed to quantitatively investigate the origins of bamboo's asymmetric characteristics, with a numerical model proposed for crack propagation. Our technique could offer microscopical insights

in the flexural failures of structural bamboo materials under bending, which may be of help on the design of advanced FG cellular composites.

Keywords Bamboo · *In situ* mechanical testing · Microstructure · Flexural behavior · Crack propagation

Introduction

Bamboo, as one of the most fastest-growing and highest-yielding natural material on Earth, has played an indispensable impact in the daily life of millions of people for centuries. In the last decades, there has been increasing interest in and research into the use of bamboo as an eco-friendly material in a wide range of applications in engineering and civil construction [1–4], such as scaffolding, bridges and fiber reinforced composites. More research efforts have been made recently in studying the mechanical properties of bamboo, such as Young's modulus [2, 5], ultimate strength [3, 6, 7] and viscoelastic behavior [8], fracture toughness [9]. For example, Dixon and Gibson [5, 10] investigated quantitatively the influence of the radial density gradient on the static mechanical properties of Moso bamboo and the results show that the volume fraction of vascular bundles is of significant importance to the mechanical properties. Obataya et al. [11] showed that the bamboo culm is quite flexible resulting from that the stiff outer layer is strained while softer inner layer is compressed, and the flexural ductility of bamboo is approximately 3.5 times compared with that of beech. Recently, Habibi and Lu [3] revealed the asymmetric flexural responses of raw bamboo (*Phyllostachys edulis*) strips using multi-scale mechanical characterizations with the assist of environmental scanning electron microscopy (ESEM). Testing data and fracture morphology suggested that the exhibited asymmetry is strongly

Electronic supplementary material The online version of this article (doi:10.1007/s40799-017-0202-5) contains supplementary material, which is available to authorized users.

✉ Y. Lu
yanglu@cityu.edu.hk

- ¹ Department of Mechanical and Biomedical Engineering, City University of Hong Kong, 83 Tat Chee Avenue, Kowloon, Hong Kong, China
- ² State Key Laboratory of Mechanics and Control of Mechanical Structures, Nanjing University of Aeronautics and Astronautics, Nanjing 210016, China
- ³ Centre for Advanced Structural Materials (CASM), City University of Hong Kong, 83 Tat Chee Avenue, Kowloon, Hong Kong, China

dependent on the gradient distribution of the vascular bundles, whereas the hierarchical fibers as well as cellular parenchyma cells (PCs) have an important influence on failure mechanisms. Despite these earlier efforts [3], so far, very few attempts [12] have been made to investigate the crack propagation behavior alongside the related mechanisms induced by bending from the point of microscale crack extension. In addition, there is also a need to develop a model by finite element method (FEM) to analysis the interior stress field of structural biomaterials with FG characteristic, such as tooth [13, 14] and nacre [15], as well as bamboo.

In addition, for in-depth understanding on the crack propagation of functionally graded materials (FGMs), innovative experimental efforts have been made, especially on developing *in situ* mechanical testing with the assist of digital image correlation (DIC) techniques. For example, Lambros et al. [16] devised a way of preparing continuous FGMs that are sensitive to the ultraviolet (UV) light, and by placing it in a UV irradiation chamber, the variation of mechanical properties can be quantitatively motored. Jain and Shukla [17] investigated on the mixed-mode dynamic fracture of FGMs based on the experiment, and found that the FGM owned a reduction of 20% density from that of the pure matrix over a distance 250 mm. As for biomaterials like bamboo, it has perfectly demonstrated the concept of FGMs where continuously graded properties are specified by spatially varying microstructure stemmed out from inter layer to outer layer [3, 18]. However, few researches paid attention to the crack propagation induced by flexural bending from the view of *in situ* testing to reveal the discrepancies in terms of crack propagation mechanisms resulted from inherent graded characteristics.

In this paper, we will mainly emphasize on developing dedicated *in situ* microscopic imaging coupled with mechanical testing system to observe the local crack propagation behavior *in situ*, rather than traditional mechanical testing with post-analysis [3], of raw bamboo strips in the course of single loading and cyclic loading. In this manner, in accordance with the snapshots directly grasped from the high-resolution telescope *in situ*, the crack initiation and propagation mechanisms in bamboo suffered from different bending configurations could be unambiguously characterized. Finally, finite element analysis was used to assist the understanding on the progression of damage induced by various bending configurations and a numerical model was proposed to understand the crack propagation in bent bamboo. We expect that these findings, along with the developed *in situ* microscopic imaging platform, could be important for understanding the toughening mechanism in other biomaterials with hierarchical structures, as well as for designing the optimum bio-inspired composites with favorable structural properties, from the *in situ* experimental perspective.

Materials and Experimental Methods

Materials and Specimen

Three-point bending experiments were conducted using the species of bamboo known as Moso or “Mao Zhu” (*Phyllostachys edulis* species, from Jiangsu and Zhejiang province in China, ~5 years old) which is one of the most commonly used species for structural purposes. In general, bamboo culm separated by nodes composes of vascular bundles, fibers and parenchyma cells [19] as shown in Fig. 1. From the Fig. 1(a), it can be obviously seen that the distribution of vascular bundles (darker color) against the lighter ground parenchyma changes continuously from the inner to the outer part along the radial direction, which actually results in a hierarchical functionally-graded characteristic of raw bamboo. Additionally, the unidirectional alignment of vascular bundles imbeds in the honeycomb-like parenchyma cells (see Figs. 1(c)–(e)), which makes the bamboo can be considered as a unidirectional reinforced functionally graded composites. Two types of bending configuration were designed and the corresponding finite element model were also established as shown in Figs. 1(f)–(h), respectively.

All of the bamboo strips cut from the middle section of stalk were prepared along the culm thickness with different fiber volume fraction, as shown in Fig. 1(a). In order to examine the size effect, two types of samples were prepared to reveal the influence of FG characteristic, shown in Fig. 1(a). The yellow solid rectangle means the cross-sectional area of bamboo strips with the size of 5.4 mm × 5.4 mm, while the white dotted rectangle represents that of bamboo strips with the size of 3.7 mm × 3.7 mm. Here, bamboo strips were firstly located into a constant drying oven (60 °C) for one day, after that exposed in the experimental environment (temperature: ~23 °C and humidity: ~55–70%) lasting 12 h.

Experimental Setup, Method and Raw Data Processing

The experimental setup for the *in situ* three-point bending tests, shown in Fig. 2, consists of a strip-shaped specimen located on the metal fixture with a support span length of 64 mm (Fig. 2(b)), a high-speed video camera (e.g. Canon™ EOS-1D X Mark II) equipped with a telephoto macro lens (Canon™ EF 100–400 mm f/4.5–5.6 L IS II USM Lens with Canon™ 77 mm 500D close-up lens attachment) linked with the remote controlling computer (with EOS Utility software) to monitor the crack growth process *in situ* (Fig. 2(c)) and a Servo-Hydraulic Axial Torsional Material Test System (Axial 5kN/ Torsional 200NM, shown in Fig. 2 (a)) to provide the quasi-static and loading/unloading loading. Additionally, in order to improve the image quality, an accessional spot-light source provided by a Motion analyzing microscope (KEYENCE™ VW-6000) was used. Once a test starts, the

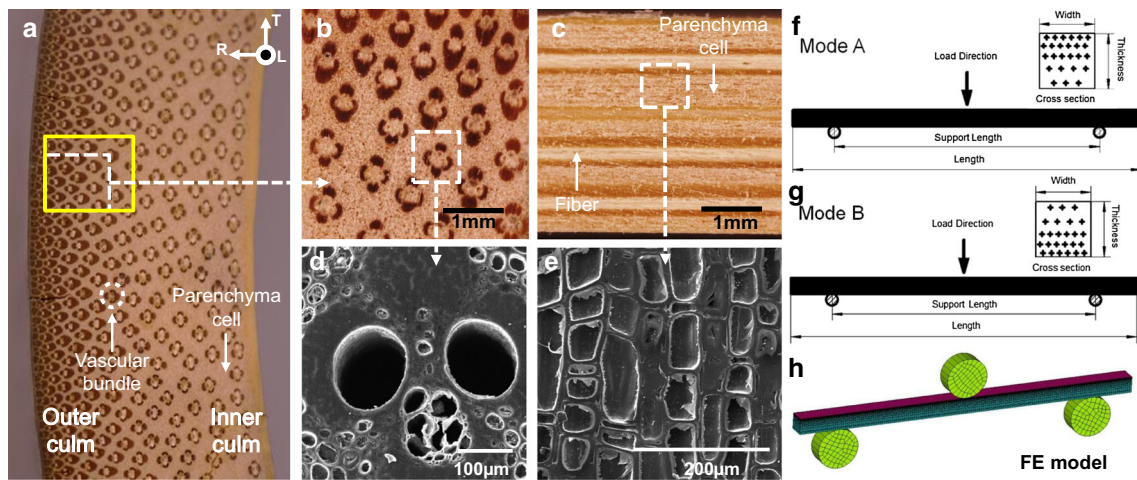


Fig. 1 Bamboo and its functional graded structure. (a) Cross-sectional area of bamboo culm in which, significantly, the amount of vascular bundles increase along the radial from inside to outside. (b)–(c) Optical macrographs of raw bamboo in the RT and TL views, respectively. (d)–(e) SEM micrographs of vascular bundles and parenchyma cell areas. (f)–(g) illustrations of bamboo strips prepared along the culm radial and the corresponding flexural bending configurations of Mode A (Loading on higher fiber density side) and Mode B (Loading on lower fiber density side); (h) Finite element (FE) model for a typical FG material which will be used to investigate the asymmetric flexural behavior

corresponding stereographic view (4096 × 2160 (4 K) or 1920 × 1080 (Full HD) pixel²) of specimen will be simultaneously recorded at 60 (up to 4 K)–120 (Full HD only) frames per second instructed by controlling system. Afterwards, local crack propagation processes captured by camera can be associated and synchronized with quantitative testing data, which provides a direct approach into the crack growth mechanism for bamboo under bending fracture.

In accordance with ASTM D79–03 (Standard Test Methods for Flexural Properties of Unreinforced and Reinforced Plastics and Electrical Insulating Materials), flexural tests include the quasi-static loading and loading/

unloading tests in the cases of Mode A (loading on higher fiber density side) and Mode B (loading on lower fiber density side). The tests were conducted by displacement control at a constant rate of 0.01 mm/s, which are fully consistent in our previous works [3]. Note that, referring to ASTM D79–03 and previous work [3], the measured parameters with respect to the displacement essentially neglect the influence of the local displacement induced by the high contact pressure of upper grip on the bamboo strips.

In order to reveal quantitatively the flexural characterization of raw bamboo, four performance indices, including flexural modulus, flexural yield strength, flexural fracture strength

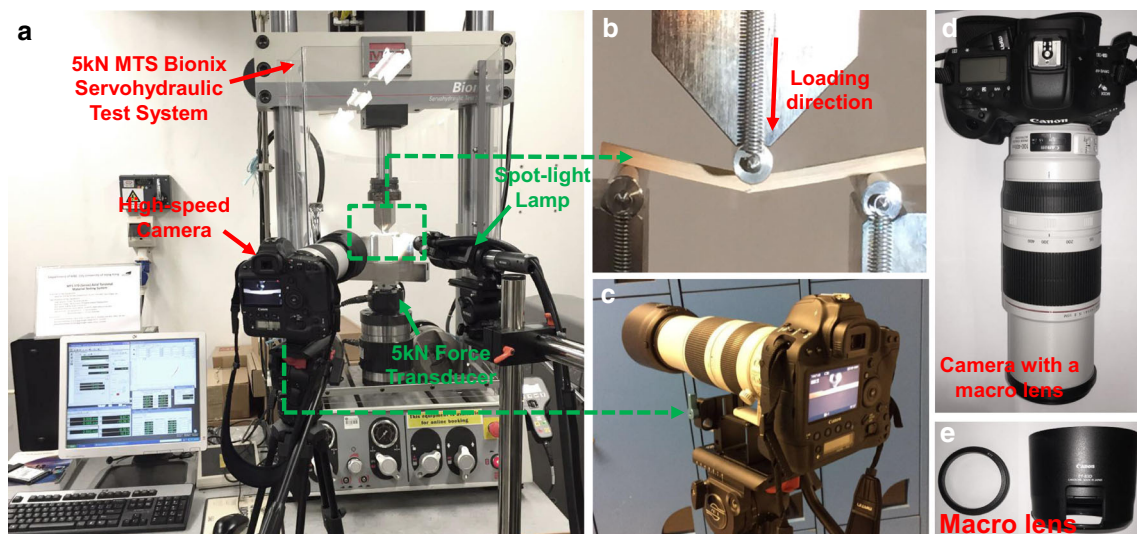


Fig. 2 Experimental setup for the *in situ* bending test with high-resolution imaging system. (a) Servo-Hydraulic Axial Torsional Material Test System with a 5kN force transducer. (b) Three-point (3-P) bending fixture. (c) *in situ* high-resolution telescope imaging system with a high-speed telescope. (d) the telescope zoom lens with (e) a macro lens attachment

and toughness, were directionally calculated or extracted from the exhibited force-deformation curves. Here, for a rectangular beam under the three-point bending, the flexural stress σ_f can be calculated by:

$$\sigma_f = \frac{3FL}{2bd^2} \quad (1)$$

where F is the load recorded by force transducer (N); L is the support span length (mm); b is the width of the specimen (mm); d is the thickness of the specimen (mm). Here, if F corresponds to the maximum loading, σ_f is generally defined as the flexural fracture strength. Herein, in accordance with the definition of yield strength in metal materials, the point from linear to nonlinear in the flexural stress-strain curves is defined as the flexural yield strength (see Fig. 3).

Flexural strain can be given by:

$$\varepsilon_f = \frac{6Dd}{L^2} \quad (2)$$

where D is the deflection of beam in accordance with the deformation of upper grip approximately (mm); L is the support span length (mm); d is the thickness of the specimen (mm). Here, if ε_f corresponds to the strain at the fracture point, it can be regarded as flexibility.

The flexural modulus, which represents the flexural modulus of elasticity, can be obtained from the following equation:

$$E_f = \frac{L^3 F}{4bd^3 D} \quad (3)$$

where D, d, L and F are the same meaning in equations (1) and (2).

Note that, due to the maximum strains in the outer surface were less than 5% (Figs. 6 and 7), the equations (1)–(3) can be reasonably adopted to estimate flexural stress and strain values in accordance with ASTM D79–03.

Results and Discussions

Previous studies [3, 11, 20] have evidenced that bamboo strips display obviously asymmetric flexural behaviors in the case of Mode A (Loading on the higher fiber density side) and Mode B (Loading on the lower fiber density side) based on the flexural testing data as well as fracture morphology analysis. In this work, the corresponding mechanical results data with respect to quasi-static three-point bending tests have been given in Table S1 in *Supplementary Information*. According to the results, bamboo strips with $3.7 \times 3.7 \text{ mm}^2$ exhibit higher flexural moduli, yield strengths and fracture strengths than those with $5.4 \times 5.4 \text{ mm}^2$ in the same bending configurations, as it is mainly attributed to the higher fiber volume fraction in the former ones. Nevertheless, due to less content in parenchyma cells for the samples with $3.7 \times 3.7 \text{ mm}^2$, the flexural toughness is diminished. In the cases of same cross-sectional size, bamboo strips demonstrate relatively larger flexural moduli and strengths (yield or fracture) in the case of Mode A compared to Mode B. Contrarily, they exhibit much larger flexural toughness in Mode B. These finds are basically consistent with our previous testing results [3].

Here, we focused on the flexural behavior (viz. single loading tests and load-unload tests) of bamboo strips with different cross-sectional sizes in the course of bending assisted with *in situ* three-point bending test platform, to visualize the crack initiation and propagation in various loading configurations.

In Situ Observation of Quasi-Static Flexural Behavior for Bamboo Strips

Based on our *in situ* testing platform, Figs. 4 and 5 show crack propagation processes for the samples with $3.7 \times 3.7 \text{ mm}^2$ and $5.4 \times 5.4 \text{ mm}^2$ cross-sectional areas in the cases of Mode A and Mode B, respectively (mechanical results data are given in Table S1 in *Supplementary Information*). Likewise, the representative three-point bending stress-strain curves of bamboo strips

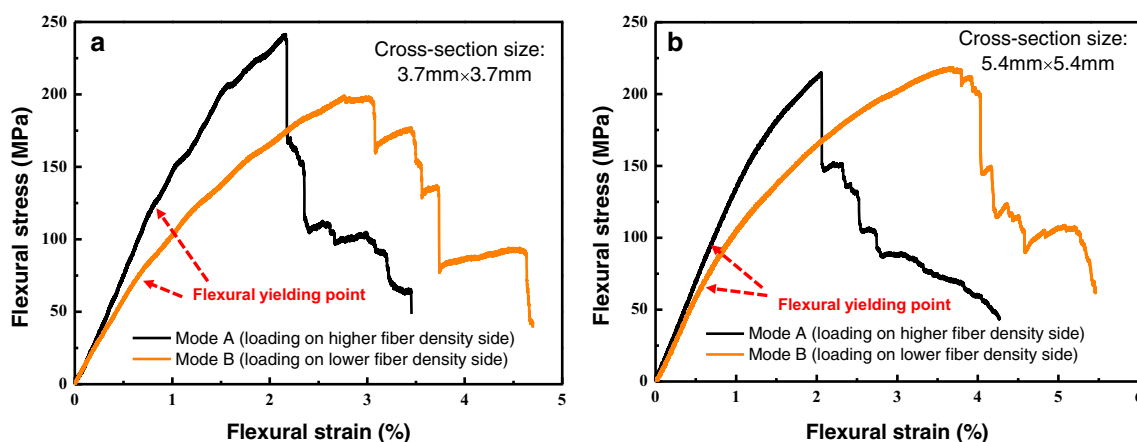


Fig. 3 Representative three-point bending stress-strain curves of bamboo strips with different cross-sectional sizes in the cases of: (a) Mode A (loading on the higher fiber density side) and Mode B (loading on the lower fiber density side) bending configurations

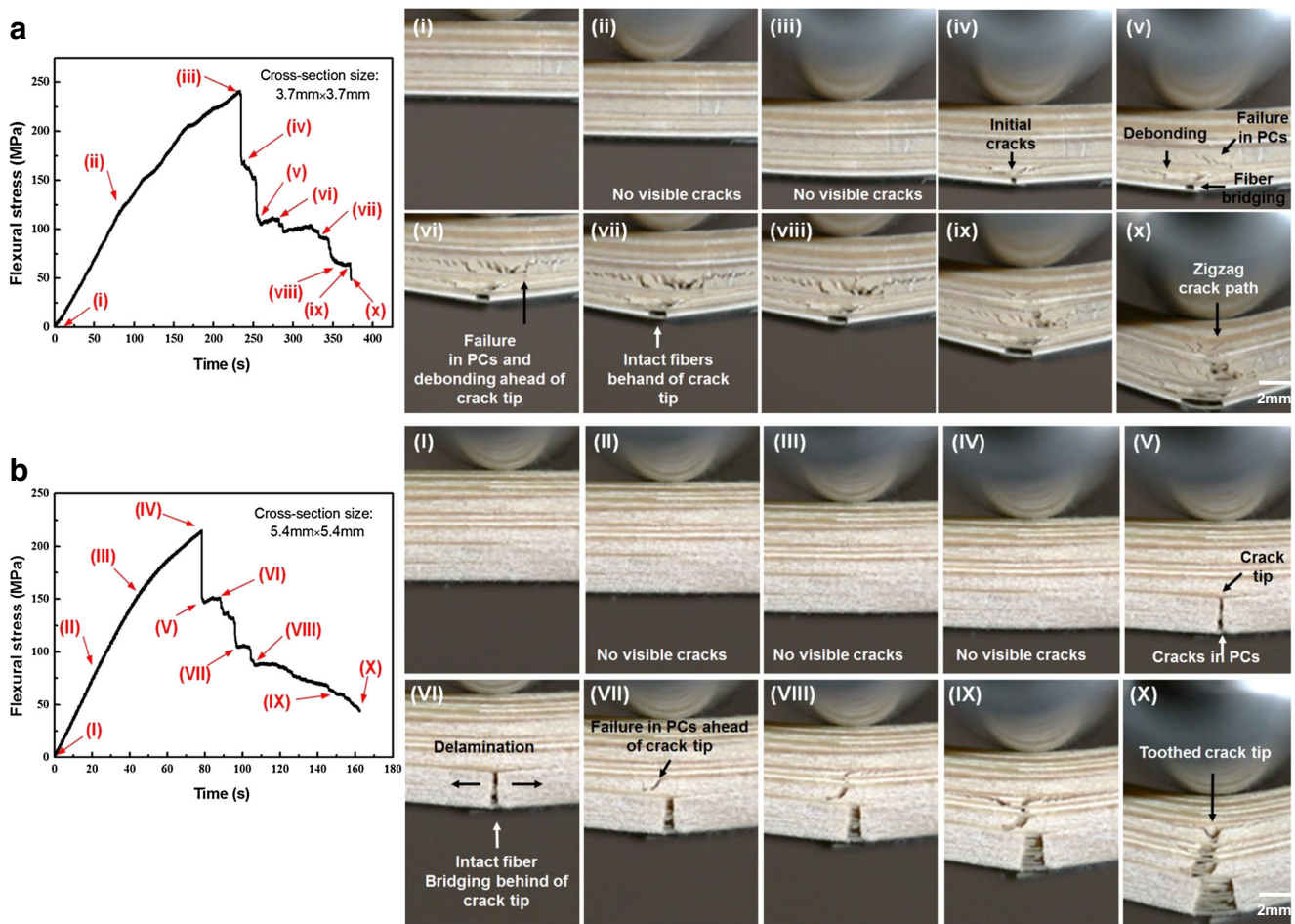


Fig. 4 Two sets of typical *in situ* three-point bending test of bamboo strips loaded on the higher fiber density side (Mode A). Here, for the sets of (a), snapshots of (i) ~ (x) correspond to the various loading times: 0 s, 90s, 230 s, 231 s, 250 s, 284 s, 324 s, 340 s, 430 s and 584 s, respectively. For the sets of (b), snapshots of (I) ~ (X) are related to the different loading times: 0 s, 24 s, 51 s, 78 s, 79 s, 88 s, 97 s, 107 s, 145 s and 163 s, respectively. We observe a characteristic fibril bridging behind the crack tip at the bottom of bamboo strip, which prevents the cracks propagation to some degree, followed by a substantial debonding phenomenon. Moreover, the crack tip gradually becomes deactivation with the zigzag configuration due to the prevention of fiber layers. Therefore, by *in situ* observation, fiber bridging and debonding are believed to induce extensive crack-deflections, resulting in efficiently relieving the stress concentration and inhibiting cracks opening, which are the main toughening mechanisms in the case of Mode A. (The typical movie for samples with $3.7 \times 3.7 \text{ mm}^2$ in the case of Mode A is given in Movies S1 in *Supplementary Information*)

with different cross-sectional sizes in Mode A and Mode B were plotted in Fig. 5. For the same sizes, it is seen that there are obvious different crack extension manners and the overall failure modes. However, for the same bending configuration, crack propagation behaviors and fracture morphology are not sensitive to the sizes of bamboo strips.

In the case of samples with $3.7 \times 3.7 \text{ mm}^2$ areas in Mode A, there was no obvious visible crack observed closed to the bottom surface, but an obvious yield phenomenon took place during the process of Fig. 4(ii)-(iii), which can be attributed to the deformation in bamboo's interior tissue, especially in foam-like parenchyma cells. Subsequently, visible cracks emerged within the bottom area in the PCs, which sharply propagated perpendicular to the bottom surface up to encountering the closest fiber layer that obstructs cracks extension.

Afterward, debonding-induced cracks were to some extent founded due to the weaker bio-chemical bond breakage [21] (Fig. 4(iii)- (v)). Interestingly, in the following process, the cracks were occurred in PCs' regions on the other side of the fiber later rather than breaking in the fiber layer, which also blunted the crack propagation path. Likewise, the fiber bridging phenomenon were truly captured with the further increase of loading, resulting in arresting the extension of cracks (Fig. 4(v)-(vi)). Hence, the crack-blunting obstructed by fiber layer, failure in PCs ahead of cracks tip and fiber bridging play a critical role in toughening behavior, inducing a characteristic zigzag crack path, which were clearly shown in Fig. 4. This mechanism continuously repeats until the ultimate failure in the case of Mode A. A similar crack extension behavior for $5.4 \times 5.4 \text{ mm}^2$ area samples were observed *in situ*, as shown in

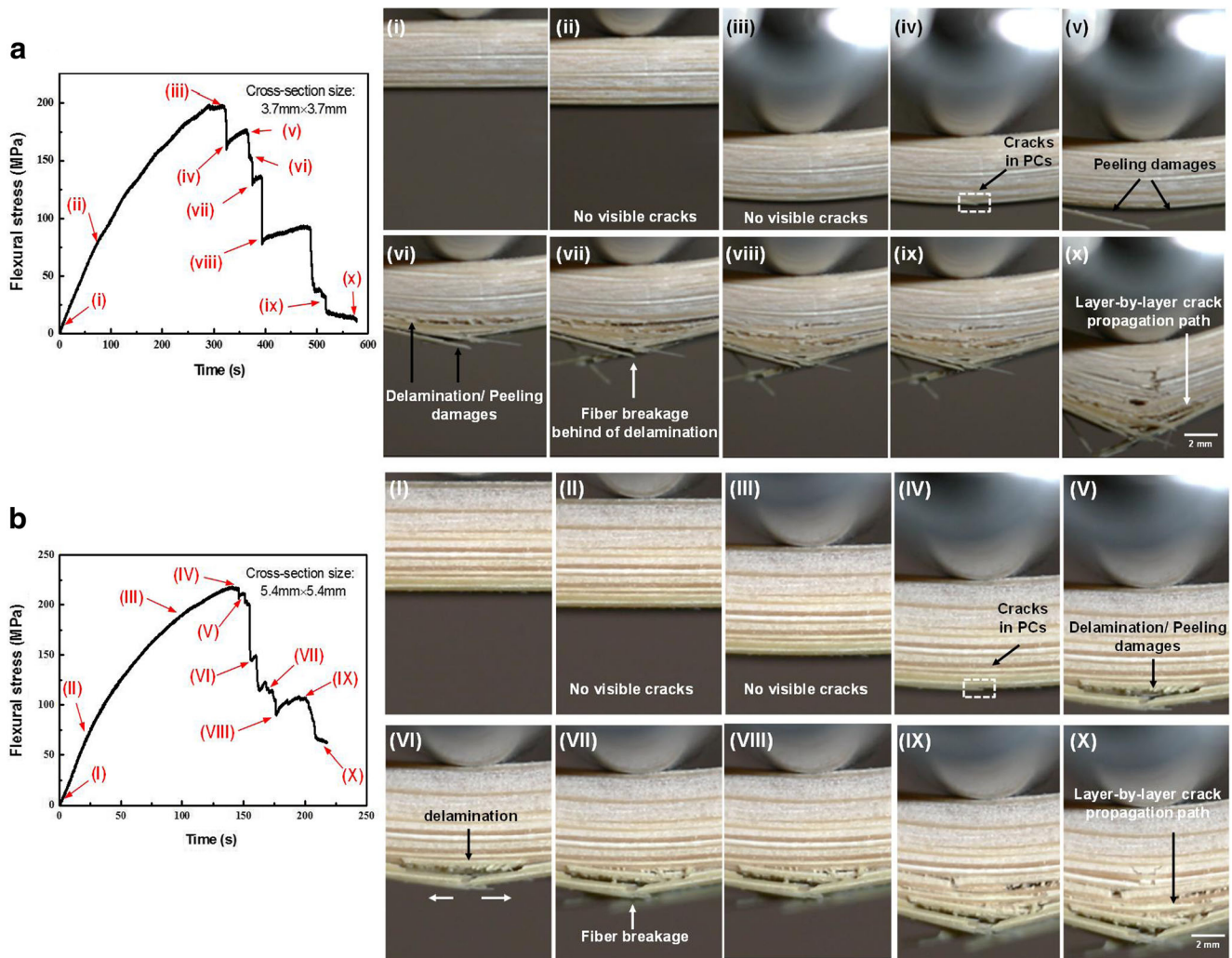


Fig. 5 *in situ* three-point bending test of bamboo loaded on the lower fiber density side (Mode B). Here, for the sets of (a), snapshots of (i) ~ (x) are related to the different loading times: 0 s, 72 s, 324 s, 325 s, 366 s, 367 s, 377 s, 394 s, 479 s and 577 s, respectively. For the sets of (b), snapshots of (I) ~ (X) correspond to the various times: 0 s, 20 s, 92 s, 145 s, 149 s, 153 s, 158 s, 162 s, 200 s and 220 s, respectively. We grasp a layer-by-layer delamination, alongside the follow-up fiber breakage, rather than fiber bridging. Such a peeling damage propagation mode by layers to a large extent blunts the movement of crack tip, which is the key toughening mechanisms of bamboo strips suffered from bending loading on the lower fiber density side. (The typical movie in the case of Mode B is given in Movies S2 in *Supplementary Information*)

Fig. 4(b). However, owing to a larger content of PCs near the bottom region, more distinctness crack propagation modes, including fiber bridging and failure in PCs region on the other side of fiber layer, were captured by *in situ* snapshots.

Compared with the crack propagation snapshots in Mode A, the corresponding illustrations recorded by *in situ* high-resolution telescope in Mode B is apparently different, irrespective of bamboo's configuration (Figs. 5(a) and (b)). Prior to the emergence of visible cracks, there were still to a large degree deformation from initial stage (i) to (iii), triggering an underlying phenomenon recorded in time-stress curve. Peeling phenomenon rather than vertical cracks propagation in PCs' area were following observed, and at the same time to some extent increase in flexural stress were obtained (Fig. 5(iv)–(v)). Afterward, the fiber/PCs interfacial delamination

developed, causing the crack propagation within the interface. When the extent of delamination reached a comparative saturation level, a large number of fiber breakages took place induced by beyond the deflection limitation of fiber layers. In the subsequent process, the crack further propagated repeatedly by the delamination, fiber breakage and failure in PCs until a catastrophic failure. As for samples with $5.4 \times 5.4 \text{ mm}^2$ area in Mode B, damage modes as well as cracks propagation behavior, viz. layer-by-layer delamination modes accompanied by following fibers breakage and PCs' failure, are practically coincident, but more obvious than those with lower cross-sectional areas (Fig. 5(b)).

To sum up, compared with the crack propagation in Mode A, the influence of fiber density distribution along the thickness on the crack propagation and the related mechanism is

remarkably different. In the case of low fiber density at the bottom side, the occurrence of crack bridging can be amplified owing to relatively large matrix spacing (Figs. 4(x) and (X)). In addition to the crack propagation manner, the degree of deformation in Mode B is obviously larger than that in Mode A according to the *in situ* snapshots (Figs. 5(x) and (X)), which can be attributed to more parenchyma density by squeezing deflection foam-like parenchyma cells in the compression zones. This microstructural characteristic coupled with layer-to-layer damage mode obstructing the movement of crack tip along the radial direction is mainly responsible for toughening mechanisms.

***In Situ* Observation of Cyclic Loading/Unloading Flexural Behavior for Bamboo Strips**

Our platform can be further extended to study the cyclic testing: generally the term of flexibility is related to the elastic behavior that the deformation can be completely recovered after the removal of the load [22]. For the raw bamboo strips, according to Figs. 4 and 5, it has clearly exhibited that bamboo strip processes an excellent capacity of deflection when it comes to three-point flexural loading. Nevertheless, it is unclear that the flexural deformation could be well recovered upon fully unloading, and whether the flexural behavior is still asymmetric during the cyclic loading-unloading process. Hence, the cyclic flexural responses, viz. underlying point and residual strain, in Mode A and Mode B were unambiguously examined by virtue of *in situ* loading-unloading three-point bending tests.

It can be clearly seen from Figs. 6(a) and (b) that although the load at each cycle was removed to zero, the unrecoverable flexural deformation, defined as “residual strain”, could not be totally recovered [Figs. 6(ii)-(vi) and (II)-(VI)]. With the increase of loading level, more significant rise in the residual strain was observed for both samples. However, during these processes, no distinct visible cracks were occurred, which reveals bamboo is not quite elastic, whereas such a large flexural deflection is attributed to the plastic deformation of its components. Because of extremely high modulus of fibers compared to that of PCs (approximate 6 times [3]) and foam-shape microstructure of PCs (Fig. 1(e)), it is therefore believed that the deflection in PCs is mainly responsible for the plastic flexural deflection phrase in the case of Mode A. It also indicates that bamboo intrinsically process an excellent characteristics of ductility.

The loading-unloading responses for the samples with $3.7 \times 3.7 \text{ mm}^2$ and $5.4 \times 5.4 \text{ mm}^2$ cross-sectional areas in Mode B were also observed *in situ*, respectively (Figs. 7(a) and (b)). Samples with different sizes exhibit similar cyclic manners, viz. residual strain and crack propagation, during the loading-unloading processes. Nevertheless, larger stress-strain hysteresis loop areas for both samples in Mode B in

comparison with those in Mode A was recorded, indicating that more strain energy can be absorb in the process of Mode B. It can be attributed that more foam-like parenchyma cells accommodate much larger plastic deflection by getting squeezed in the compressively deformed parts of the strips in the top layer of Mode B than that of Mode A [3]. In addition to the aspect of residual strain, the crack extension behaviors during the cyclic loading were in general similar with those in the corresponding bending configuration during the quasi-static loading, indicating that similar toughening mechanisms with respect to each cycle still exist in the corresponding cyclic process.

Finite Element Analysis of Asymmetric Bending Prior to the Initial Crack

Our *in situ* testing platform can provide an effective approach to insight the crack propagation behavior with the aim of revealing the corresponding damage mechanisms, but it cannot provide directly mechanism why such a difference in crack initiation between the loading on the higher fiber density side and the lower one. Consequently, to assist *in situ* testing results and visualize the analysis prior to the crack propagation, the internal stress fields of FG materials induced by flexural loading in the case of Mode A and Mode B was numerically simulated using the finite element analysis (FEA, ANSYS™, 14.5). The finite element models, shown in Fig. 1(h), with length 84 mm, height of 3.7 mm and thickness of 3.7 mm were adopted in the simulation, where the displacement of downside two circular configuration that represents the rigid clamp were completely fixed, and the “-Y” axis displacement load was by constant incremental step applied to the upside circular structure (coordinate system refers to Fig. 8). In addition to the load, three sets of contact pairs between the circular configurations and rectangular configuration that represents bamboo strip were established to transmit the load. In order to be closed to the truly internal structure of bamboo strip, here, the simulation modes shown in Figs. 8(a) and (b) were long-fiber-reinforced functionally graded composites, yet the distributional regular for the fibers was totally opposite. An 8-node quadrilateral element type with 3.7 mm thickness was assigned to each member. To simulate precisely the mechanical behavior of bamboo, the modulus of reinforced fibers (“red” part in Fig. 1(h)) and matrix (“green” part in Fig. 1(h)) are 22.8GPa and 3.7GPa, both of which refer to the corresponding modulus of bamboo fiber and parenchyma cells, respectively [23]. The mechanical behavior of fixture was accordant with that of steel.

As represented by the “X” stress contour, the overall stress distributions in the different bending configuration were remarkably distinct, in particular near the downside and upside surfaces. Although the maximum stress still occurred in the lowest fiber layer (~109 MPa for Mode

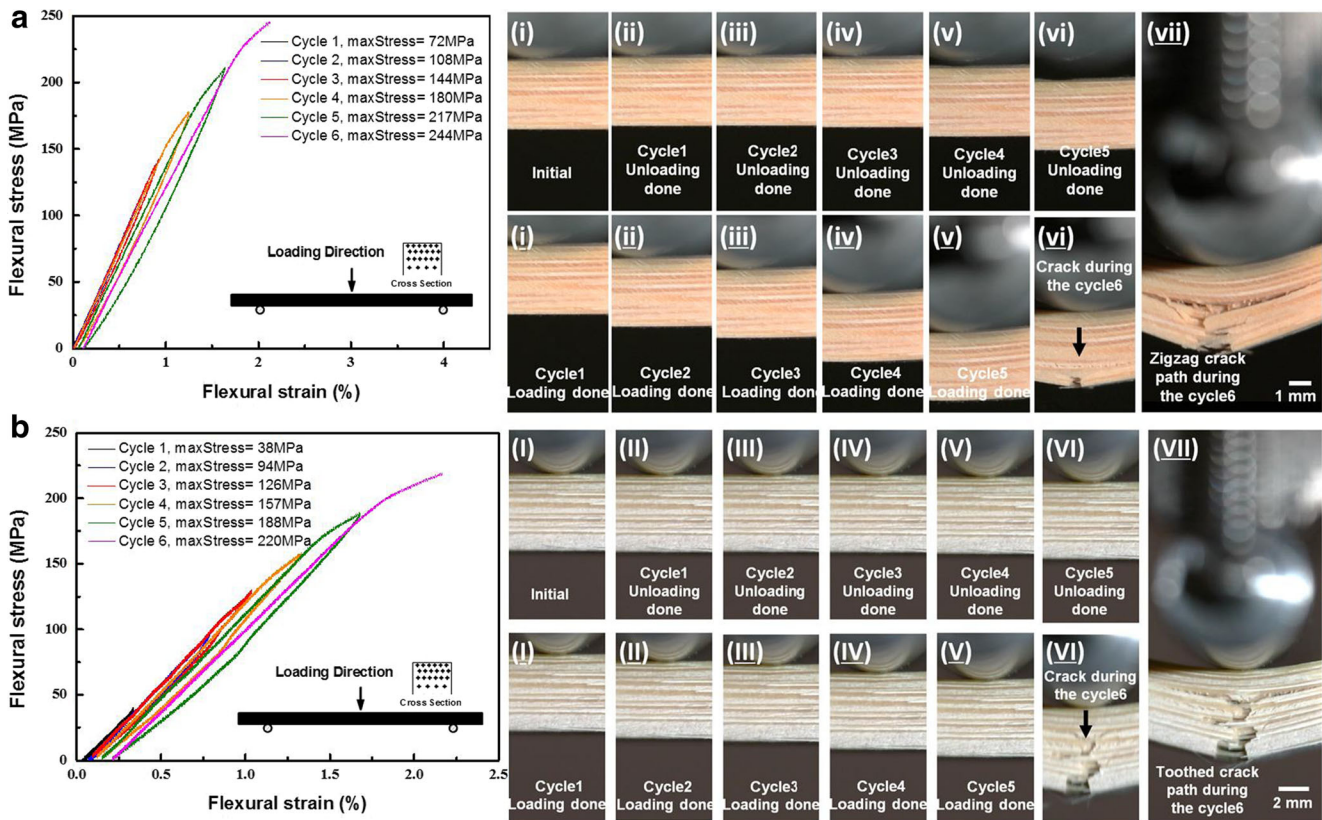


Fig. 6 *in situ* loading-unloading processes for samples with $3.7 \times 3.7 \text{ mm}^2$ areas (a) and $5.4 \times 5.4 \text{ mm}^2$ areas (b) subjected to flexural loading in the case of Mode A. For the sets of (a), snapshots of (i) ~ (iv) involve that initial state and end states at the 1st ~ 5th unloading cycle, respectively. Snapshots of (i) ~ (v) are related to accomplishment states at the 1st ~ 5th loading cycle, while *in situ* photos of (vi) and (vii) display the crack propagation and failure states. For the sets of (b), snapshots of (I) ~ (VI) refer to the initial state and end state at the 1st ~ 5th unloading cycle, respectively. Snapshots of (I) ~ (V) are related to the end states at 1st ~ 5th loading cycle, while *in situ* photos of (VI) and (VII) are associated with the states crack growth (VI) and at the end of cyclic test (VII)

A, ~105 MPa for Mode B), the stress level of matrix in the case of Mode A was higher than that in the case of Mode B, with values of 57.1 MPa and 42.7 MPa, respectively. Moreover, the orange area for Mode A was clearly larger than that for Mode B, resulting in a larger extent matrix failure tendency to be emerged in the former case, followed by forming a fiber-bridging mode to arrest the structural deformation as well as crack propagation. However, fiber breakage mode may occur prior to the matrix failure mode in the case of Mode B as the higher local stress in fiber closed to bottom side, which can be further trigger the peeling and delamination damage induced by tensile-shear stress. On the other hand, obvious compressive stress state closed to the upside surface were formed in both cases, which can inevitably lead to the flexural deformation, especially in the area of matrix. Such a flexural deformation can be regarded as the key reason that triggers plastic behaviors in the both stress-strain curves (see Figs. 4 and 5) and residual strain during the load-unload cycles (see Figs. 6 and 7). More

exactly, the maximum of compressive stress in Mode A was nearly two times as large as that in Mode B, meaning that compression-induced plastic deformation in matrix tend to be occurred in the former case. Whereas, the regions controlled by compressive stress in Mode B are larger than that in Mode A, which may be attributed to the more matrix that can absorb the strain energy by deformation acts near the upside surface.

Crack Propagation Model

Tortuous crack growth [20] along the radial (“R”) and longitudinal (“L”) directions (see Fig. 1) is significantly relevant to the microstructure of bamboo strips (see Figs. 4 and 5), a geometry-dependent model initially proposed by Hanlon et al. [24] can be adopted to quantitatively estimate the state of crack propagation in bamboo. In accordance with the *in situ* snapshots shown in Figs. 4 and 5, zigzag crack growth mode induced by crack tips’ interaction with hollow vessels and interfacial failure

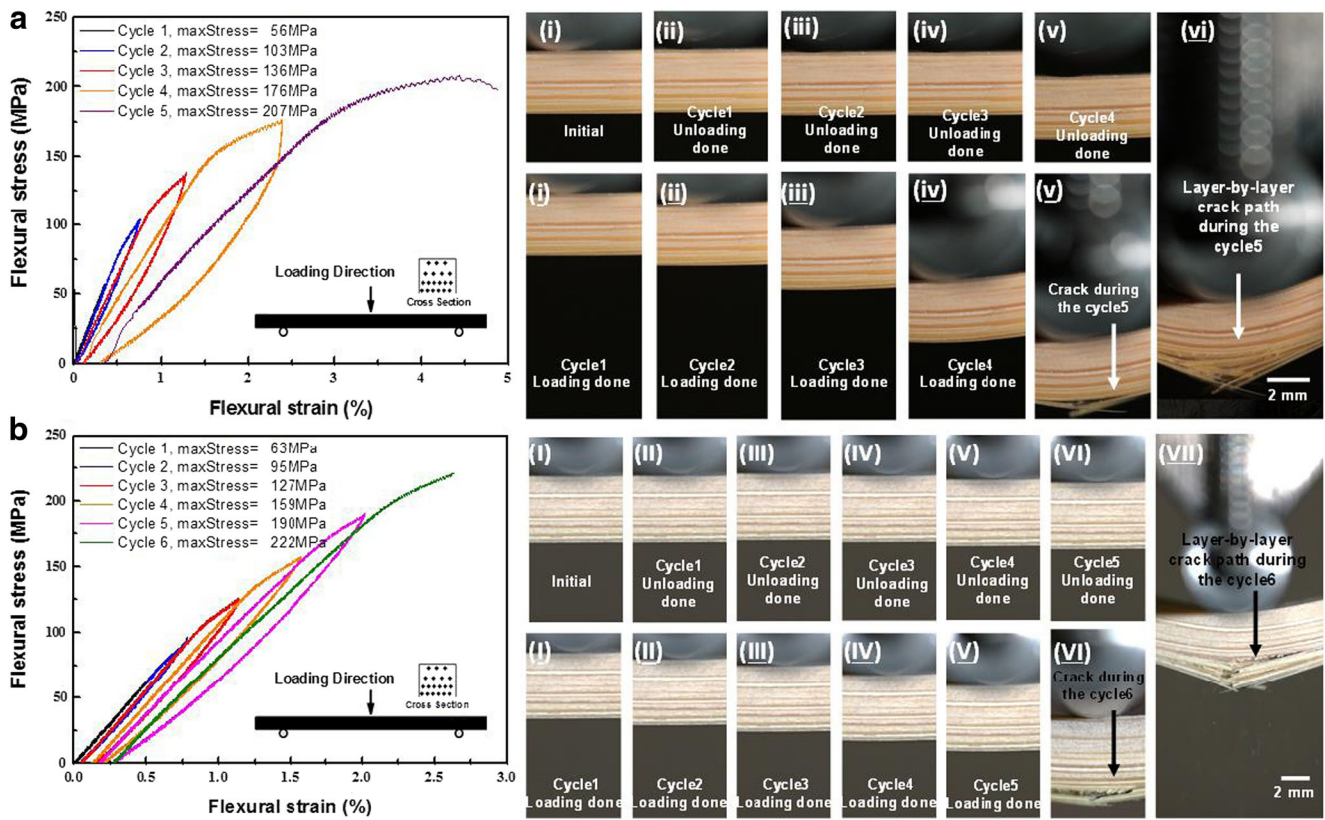


Fig. 7 *in situ* loading-unloading processes for samples with $3.7 \times 3.7 \text{ mm}^2$ areas (a) and $5.4 \times 5.4 \text{ mm}^2$ areas (b) subjected to flexural loading in the case of Mode B. For the sets of (a), snapshots of (i) ~ (iv) correspond to initial state and end state at the 1st, 2nd, 3rd and 4th unloading cycle, respectively. Snapshots of (i) ~ (iii) are related to accomplishment state at the 1st, 2nd and 3rd loading cycle, while *in situ* photos of (iv) ~ (vii) mean that the state prior to the emerge of visible damage (iv), during the crack propagation (v) ~ (vi) and at the end of cyclic test (vii). For the sets of (b), snapshots of (I) ~ (VI) refer to the initial state and end state at the 1st ~ 5th unloading cycle, respectively. Snapshots of (I) ~ (V) are related to the end state at 1st ~ 5th loading cycle, while *in situ* photos of (VI) and (VII) are associated with the state ahead of the occurrence of damage (VI) and at the end of cyclic test (VII). (The typical movie for the samples with $3.7 \times 3.7 \text{ mm}^2$ in the case of Mode B is given in Movies S3 in Supporting Information)

mechanisms could be assumed that the crack linked at an average angle inclined θ with respect to the mode I plane. Here, it is assumed that the bamboo strips mostly experiences the mode I crack opening (“R” direction, see Fig. 1(a)), and any deviation of the crack away from the mode I growth plane leads to a mixed loading mode at the tip the crack. Therefore, the local effective stress intensity factor at the tip of the crack considering the crack growth in both “R” and “L” could be then approximated by[24]:

$$K_{eff} = \cos^2\left(\frac{\theta}{2}\right)K_I \tag{4}$$

where K_I means the straight crack growth along the “R” direction. According to the results[20] and in view of the exhibited microstructure of deformed bamboo microstructures (see Fig. S1 in *Supplementary Information*), the

average inclined angle θ_R along “R” direction induced by occurrence of interfacial fracture among parenchyma cells and fibers could be estimated by geometric configuration:

$$K_{eff}^C(R) = \begin{cases} (0.75\sim 0.95)K_I^C(\theta \in [25^\circ, 60^\circ], Cc\text{Parenchyma cell}) \\ (0.75\sim 0.85)K_I^C(\theta \in [45^\circ, 60^\circ], Cc\text{Fiber}) \end{cases} \tag{5}$$

Likewise, in the “L” direction, the effective stress intensity factors could be estimated to be:

$$K_{eff}^C(L) = \begin{cases} 0.5K_I^C(\theta \sim 90^\circ, Cc\text{Parenchyma cell}) \\ 0.5K_I^C(\theta \sim 90^\circ, Cc\text{Fiber}) \end{cases} \tag{6}$$

Herein, for a rectangular plate with the width of W , containing a through-thickness single edge crack of length a , it is

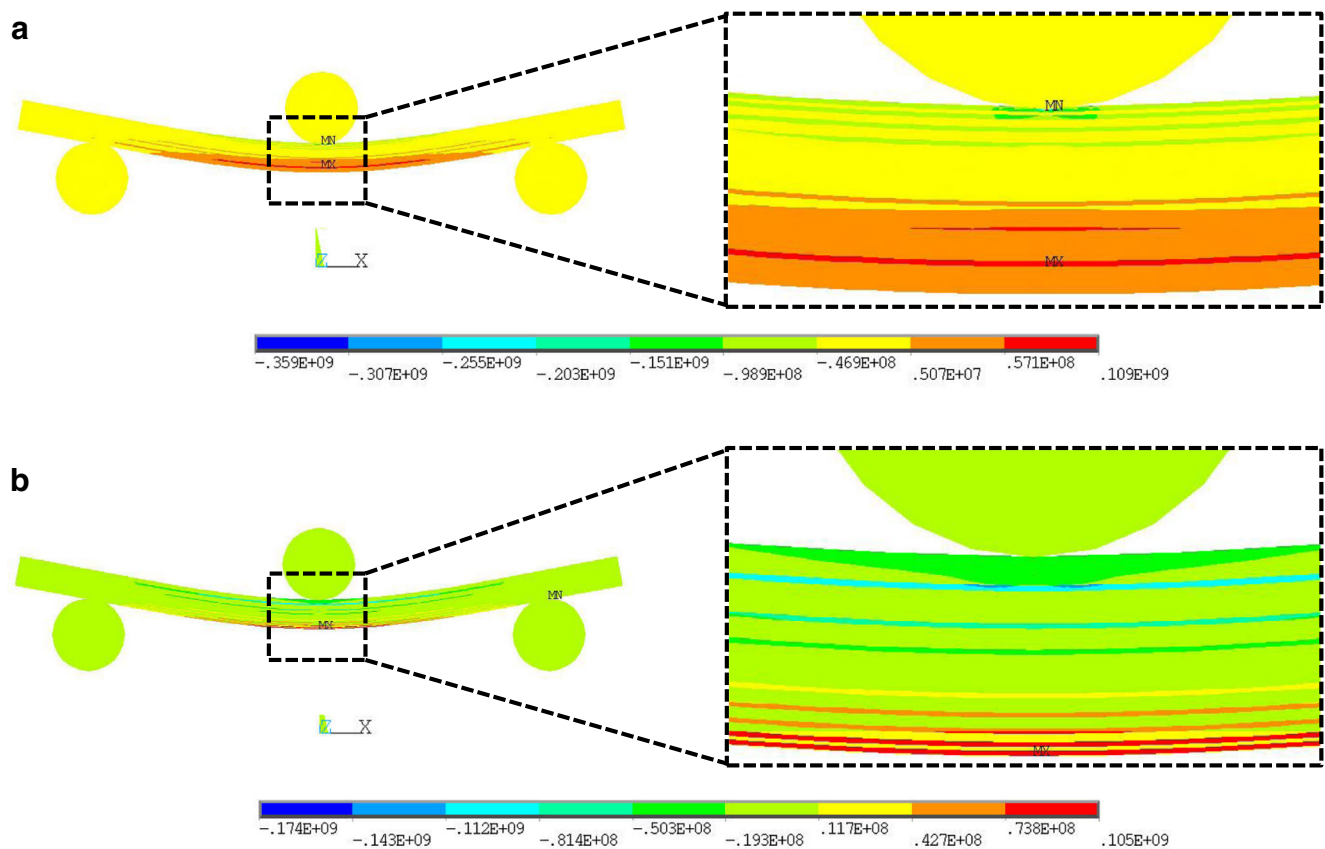


Fig. 8 Finite element (FE) analysis for functionally graded unidirectional reinforced composites subjected to different bending configurations: (a) Mode A and (b) Mode B loading simulations

commonly known that the stress intensity factor can be expressed by [24]:

$$K_I = \sigma \sqrt{a} f\left(\frac{a}{W}\right),$$

$$f\left(\frac{a}{W}\right) = 1.99 - 0.41\left(\frac{a}{W}\right) + 18.7\left(\frac{a}{W}\right)^2 - 38.48\left(\frac{a}{W}\right)^3 + 53.85\left(\frac{a}{W}\right)^4 \quad (7)$$

Although the different stress intensity factors K_{eff} between bamboo and polycrystalline solid [24], the combined effect according to aforementioned estimations and their interplays is similar, which will result in an overall reduction of the driving force for crack propagation in the whole bamboo structure [20].

To account for the extra crack length accrued during deflection, the modified crack growth rate can be expressed as follows [25, 26]:

$$\left(\frac{da}{dF}\right) = A \left(\frac{D \cos \theta + S}{D + S}\right)^\lambda K_{eff}^m \quad (8)$$

where the deflected cracks are assumed to comprise a nominally straight segment of length S , oriented parallel to the

initial crack direction, and a kinked segment, of length D , inclined at an angle, θ ; F means external loading; A and λ are the correlation coefficient. Therefore, the relationship between crack growth rate (da/dF) and the stress intensity factors K_{eff} can be quantitatively established.

In fact, a propagating crack affected by such interactions amongst the geometric configuration has been likewise found in other plant tissues. For instant, in wood, crack propagation often occurs by the delamination of earlywood, which causes deflection around the cells, and is arrested as it approaches the latewood layers [27]. In serrated leaf, the stress field at the root of a notch in leaf will be distorted in nonlinear proportion to the prevailing direction of fibrous reinforcement, and the fracture toughness can be estimated by three crack modes, viz. opening (mode I, K_I), sliding (mode II, K_{II}) and tearing (mode III, K_{III}), respectively [28].

Conclusion

In this work, quasi-static and cyclic bending flexural behaviors of structural bamboo materials were characterized by our *in situ* three-point bending test platform. To understand the

mechanisms for the asymmetric fracture behavior during the processes of crack initiation and propagation, a finite element model in term of functionally graded materials was established to assist the experimental observation to reveal the internal stress distribution characteristic in different bending configurations. As shown in the *in situ* microscopic imaging, bamboo strips exhibit distinct asymmetric crack propagation manners induced by the FG hierarchical microstructure during the quasi-static loading and cyclic loading/unloading processes. Moreover, the loading/unloading *in situ* images unambiguously reveal that bamboo strips own a unique elastic-plastic flexural characteristic, which should attribute to the foam-like parenchyma cells. By learning from bamboo's hierarchical cellular structure during real-time deformation, it is possible to mimic the structure-property relationship and structural behavior of natural materials to develop novel bio-inspired composites for various engineering applications.

Acknowledgments The authors gratefully thank Bing Chen and Prof. Xinrui Niu at City University of Hong Kong for the instrumental support and discussions. This work was supported by City University of Hong Kong under the ARG grants # 9667117, # 9667153 and project # 6000604 and #9610288.

Compliance with Ethical Standards

Conflict of Interest The authors have no competing interests in this work.

References

- Liese W, Kohl M (2015) Bamboo. Springer, Switzerland
- Tan T, Rahbar N, Allameh S, Kwofie S, Dissmore D, Ghavami K, Soboyejo W (2011) Mechanical properties of functionally graded hierarchical bamboo structures. *Acta Biomaterialia* 7:3796–3803
- Habibi MK, Samaei AT, Gheshlaghi B, Lu J, Lu Y (2015) Asymmetric flexural behavior from bamboo's functionally graded hierarchical structure: underlying mechanisms. *Acta Biomaterialia* 16:178–186
- Nurdiah EA (2016) The Potential of Bamboo as Building Material in Organic Shaped Buildings. *Procedia-Soc Behav Sci* 216:30–38
- Dixon PG, Gibson LJ (2014) The structure and mechanics of Moso bamboo material. *J R Soc Interface* 11(20):140–321
- Shao Z-P, Fang C-H, Huang S-X, Tian G-L (2010) Tensile properties of Moso bamboo (*Phyllostachys pubescens*) and its components with respect to its fiber-reinforced composite structure. *Wood Sci Technol* 44:655–666
- Chen H, Cheng H, Wang G, Yu Z, Shi SQ (2015) Tensile properties of bamboo in different sizes. *J Wood Sci* 61:552–561
- Habibi MK, L-h T, Lau D, Lu Y (2016) Viscoelastic damping behavior of structural bamboo material and its microstructural origins. *Mech Mater* 97:184–198
- Amada S, Untao S (2001) Fracture properties of bamboo. *Compos Part B Eng* 32:451–459
- Dixon P, Semple K, Kutnar A, Kamke F, Smith G, Gibson L (2016) Comparison of the flexural behavior of natural and thermo-hydro-mechanically densified Moso bamboo. *Eur J Wood Wood Prod* 74(5):633–642
- Obataya E, Kitin P, Yamauchi H (2007) Bending characteristics of bamboo (*Phyllostachys pubescens*) with respect to its fiber-foam composite structure. *Wood Sci Technol* 41:385–400
- Askarinejad S, Kotowski P, Youssefian S, Rahbar N (2016) Fracture and mixed-mode resistance curve behavior of bamboo. *Mech Res Commun* 78:79–85
- Niu X, Soboyejo W (2006) Effects of loading rate on the deformation and cracking of dental multilayers: Experiments and models. *J Mater Res* 21:970–975
- Niu X, Yang Y, Soboyejo W (2008) Contact deformation and cracking of zirconia/cement/foundation dental multilayers. *Mater Sci Eng: A* 485:517–523
- Barthelat F, Li C-M, Comi C, Espinosa HD (2006) Mechanical properties of nacre constituents and their impact on mechanical performance. *J Mater Res* 21:1977–1986
- Lambros J, Santare M, Li H, Sapna G III (1999) A novel technique for the fabrication of laboratory scale model functionally graded materials. *Exp Mech* 39:184–190
- Jain N, Shukla A (2006) Mixed mode dynamic fracture in particulate reinforced functionally graded materials. *Exp Mech* 46:137–154
- Silva ECN, Walters MC, Paulino GH (2006) Modeling bamboo as a functionally graded material: lessons for the analysis of affordable materials. *J Mater Sci* 41:6991–7004
- Schaedler TA, Jacobsen AJ, Torrents A, Sorensen AE, Lian J, Greer JR, Valdevit L, Carter WB (2011) Ultralight metallic microlattices. *Science* 334:962–965
- Habibi MK, Lu Y (2014) Crack propagation in bamboo's hierarchical cellular structure. *Sci Rep* 4:5598
- Mwaikambo LY, Ansell MP (2002) Chemical modification of hemp, sisal, jute, and kapok fibers by alkalization. *J Appl Polym Sci* 84:2222–2234
- Shah DU, Schubel PJ, Clifford MJ, Licence P (2012) The tensile behavior of off-axis loaded plant fiber composites: An insight on the nonlinear stress-strain response. *Polym Compos* 33:1494–1504
- Amada S, Ichikawa Y, Munekata T, Nagase Y, Shimizu H (1997) Fiber texture and mechanical graded structure of bamboo. *Compos Part B Eng* 28:13–20
- Hanlon T, Tabachnikova E, Suresh S (2005) Fatigue behavior of nanocrystalline metals and alloys. *Int J Fatigue* 27:1147–1158
- Suresh S (1985) Fatigue crack deflection and fracture surface contact: micromechanical models. *Metall Mater Trans A* 16:249–260
- Granacher J, Klenk A, Tramer M, Schellenberg G, Mueller F, Ewald J (2001) Creep fatigue crack behavior of two power plant steels. *Int J Press Vessel Pip* 78:909–920
- Valentin G, Adjanohoun G (1992) Applicability of classical isotropic fracture mechanics specimens to wood crack propagation studies. *Mater Struct* 25:3–13
- Farquhar T, Zhao Y (2006) Fracture mechanics and its relevance to botanical structures. *Am J Bot* 93:1449–1454